



Article

Thermoelectric Characteristics of A Single-Crystalline Topological Insulator Bi₂Se₃ Nanowire

Dedi ^{1,2,*}, Ping-Chung Lee ², Pai-Chun Wei ³ and Yang-Yuan Chen ²

¹ Research Center for Electronics and Telecommunications (P2ET), Indonesian Institute of Sciences (LIPI), Bandung 40135, Indonesia

² Institute of Physics, Academia Sinica, Taipei 11529, Taiwan; plexlee@gmail.com (P.-C.L.); chen2@phys.sinica.edu.tw (Y.-Y.C.)

³ Center for Condensed Matter Sciences and Center of Atomic Initiatives for New Materials, National Taiwan University, Taipei 10617, Taiwan; pcwei68@gmail.com

* Correspondence: dedi030@lipi.go.id; Tel.: +62-22-250-4660

Abstract: The discovery of topological insulators (TIs) has motivated detailed studies on their physical properties, especially on their novel surface states via strong spin–orbit interactions. However, surface-state-related thermoelectric properties are rarely reported, likely because of the involvement of their bulk-dominating contribution. In this work, we report thermoelectric studies on a TI bismuth selenide (Bi₂Se₃) nanowire (NW) that exhibit a larger surface/volume ratio. Uniform single-crystalline TI Bi₂Se₃ NWs were successfully synthesized using a stress-induced growth method. To achieve the study of the thermoelectric properties of a nanowire (NW), including electrical conductivity (σ), Seebeck coefficient (S), and thermal conductivity (κ), a special platform for simultaneously performing all measurements on a single wire was designed. The properties of σ , S , and κ of a 200 nm NW that was well precharacterized using transmission electron microscope (TEM) measurements were determined using the four-probe method, the two-probe EMF across ∇T measurement, and the 3ω technique, respectively. The integrated TE properties represented by the figure of merit ZT ($S^2\sigma T/\kappa$) were found to be in good agreement with a theoretical study of Bi₂Se₃ NW.

Keywords: thermoelectric; bismuth selenide; nanowire



Citation: Dedi; Lee, P.-C.; Wei, P.-C.; Chen, Y.-Y. Thermoelectric Characteristics of A Single-Crystalline Topological Insulator Bi₂Se₃ Nanowire. *Nanomaterials* **2021**, *11*, 819. <https://doi.org/10.3390/nano11030819>

Academic Editor: Matthias Elm

Received: 21 February 2021

Accepted: 20 March 2021

Published: 23 March 2021

Publisher's Note: MDPI stays neutral with regard to jurisdictional claims in published maps and institutional affiliations.



Copyright: © 2021 by the authors. Licensee MDPI, Basel, Switzerland. This article is an open access article distributed under the terms and conditions of the Creative Commons Attribution (CC BY) license (<https://creativecommons.org/licenses/by/4.0/>).

1. Introduction

The study of nanoengineered thermoelectric materials used for converting waste heat into electricity has become a compelling research topic [1–5]. The thermoelectric (TE) generator and the TE sensor are devices that can harvest renewable energy for power generation and thermal sensing, respectively [6–11]. The efficiency of TE materials is determined by the dimensionless figure of merit ZT , which is defined as $S^2\sigma T/(\kappa_e + \kappa_l)$, where S is the TE power or Seebeck coefficient, σ represents the electrical conductivity, κ_e is the electronic thermal conductivity, and κ_l is the lattice thermal conductivity. The quantity $S^2\sigma$ is defined as the power factor (PF). The Weidmann–Franz law restricts the ratio σ/κ in a bulk TE compound. Furthermore, a sharply peaked density of states (DOS) favors a large S , while the density of states in bulk materials is a smoothly variable function. As dimensionality is reduced from three to one, the electronic DOS at the energy-band edges is significantly increased, increasing the TE PF ($S^2\sigma$) and yielding an improved ZT [12,13]. Then, according to Dresselhaus et al., 1D nanowires can boost thermoelectric performance [13,14]. A Bi nanowire would also have a reduced κ due to phonon scattering off the sidewalls, which helps increase ZT , based on a previous study [13,15].

Slack et al. reported that semiconductors exhibiting narrow band gaps and high mobility carriers are optimal TE materials [16]. Bi₂Se₃ is a V–VI topological-insulator material that exhibits a narrow band gap of approximately 0.3 eV and crystallizes in a rhombohedral structure belonging to the tetradymite space group D_{3d}^5 (R-3m) [17–19]. This

material demonstrates potential for application in optical recording systems [20], photo-electrochemical devices [21], and TE devices [17,18]. In recent years, bismuth chalcogenides have attracted substantial research interest because of their superior TE properties of high ZT at room temperature [22]. Diverse synthesis techniques have been developed to synthesize various nanostructures of Bi_2Se_3 , such as microwave heating [23,24], a single-source precursor method [25–27], solvothermal method [28–30], the metal–organic chemical vapor deposition method [31,32], and mechanical exfoliation [33–35], whereas the commonly used synthesis method for producing Bi_2Se_3 bulk single-crystalline material is based on the Bridgman technique [36–41]. However, only a few studies have been reported on growing Bi_2Se_3 NWs and characterizing their TE properties.

2. Materials and Methods

We previously synthesized PbTe NWs from a PbTe thin film (TF) on a SiO_2/Si substrate using a stress-induced method [42,43] based on a mechanism in which mismatched thermal expansion between a substrate and deposited film drove the mass flow along grain boundaries at thermal annealing temperatures. This innovative NW-growth method (which does not involve conventional templates, catalysts, or starting materials) enables us to control growth conditions for growing different diameters, shapes, and aspect ratios of single-crystalline NWs [44,45], thus enabling exploration of any possible novel TE property of Bi_2Se_3 NWs.

The starting Bi_2Se_3 crystalline ingot was synthesized from Bi and Se source materials using the Bridgman method. Bi (99.999%, –200 mesh, Alfa Aesar, Lancashire, UK) and Se (99.999%, –200 mesh, Alfa Aesar, Lancashire, UK) powders were first mixed at a 2:3 ratio and then melted at 800 °C for 4 h in a vacuumed quartz tube at a pressure less than 5×10^{-6} torr. The molten compound was slowly cooled in the furnace to room temperature. Subsequently, a pellet specimen cut from the compound served as the target for pulsed laser deposition (PLD). Single-crystal SiO_2/Si (100) wafers (E-light Tech. Inc. Taipei, Taiwan; SiO_2 thickness = 1 μm ; diameter = 100 ± 0.5 mm) with double-side polishing were cut into 1.5×1.5 cm² squares for substrates. All substrates were cleaned using acetone, isopropyl alcohol, and deionized water in an ultrasonic bath for 10 min before being dried with an N_2 stream. The Bi_2Se_3 films were fabricated using an ArF excimer laser (Lambda Physik LPXPro 210, Santa Clara, California, USA) and deposited onto substrates in a vacuum system with a base pressure of 5.0×10^{-7} torr. The Bi_2Se_3 TFs were grown at a deposition rate of 0.3 Å/s, and the excimer laser was applied at 140 mJ (frequency = 10 Hz) for 15 min at room temperature. The substrate was rotated at approximately 10 rpm, and the film thickness was 30 nm. The films were sealed in a vacuumed quartz tube at less than 5×10^{-6} torr for annealing at 450 °C for 5 d, followed by cooling the furnace to room temperature. During the annealing process, Bi_2Se_3 NWs grew from the film via the different thermal expansion coefficients of the Bi_2Se_3 film ($19 \times 10^{-6}/^\circ\text{C}$) [46] and the SiO_2/Si substrate ($0.5 \times 10^{-6}/^\circ\text{C}$)/($2.4 \times 10^{-6}/^\circ\text{C}$) [42–45].

3. Results and Discussion

3.1. Characterization of Materials

Field emission scanning electron microscopy (Hitachi Co., S-4800, Tokyo, Japan) images of the Bi_2Se_3 NWs (Figure 1a) showed that the NWs exhibited diameters ranging from 50 to 500 nm and lengths up to 100 μm . Straight and uniform Bi_2Se_3 NWs of high aspect ratio grew on the substrate after annealing. A tungsten needle ($d = 100$ nm) and a binocular optical microscope were used to extract a single-crystal NW from the Bi_2Se_3 film; the NW was then suspended on a Si_3N_4 microchip by using electrodes (Figure 1b) and employed in structural analyses and thermoelectricity measurements. A transmission electron microscope (TEM; JEOL JEM-2100 at 200 kV, Tokyo, Japan) was used to examine the crystalline structure of the Bi_2Se_3 NW (Figure 1c,d).

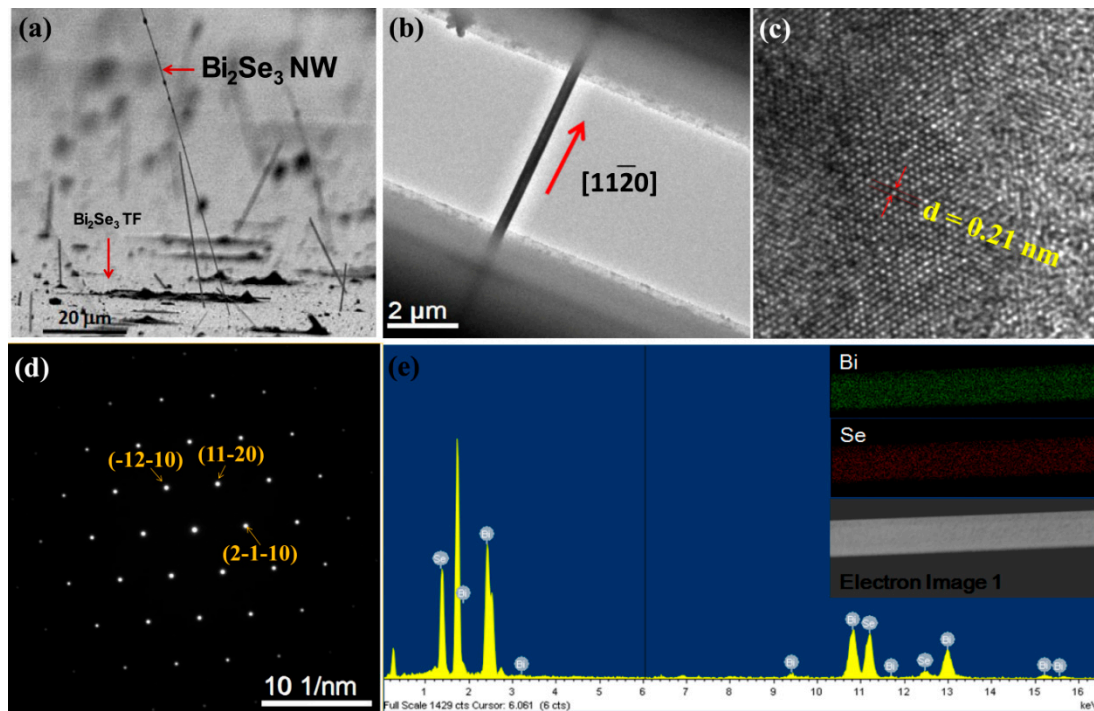


Figure 1. (a) SEM image (top view) indicating that all Bi_2Se_3 NWs grew several micrometers in length from the surface of the Bi_2Se_3 TF; (b) TEM images of a single-crystal Bi_2Se_3 NW suspended on a Si_3N_4 microchip following electrode formation by using a FIB that served as the TEM holder; (c) HR-TEM image of the NW shown in (b), where the distance between crystal faces is 0.21 nm; (d) the SAED pattern (at the $[0001]$ zone axis), confirming that the single-crystalline NWs grew in the $[11\bar{2}0]$ direction; and (e) EDS spectrum of a Bi_2Se_3 NW (the inset shows the EDS mapping image of a NW).

The electrical resistivity ρ and Seebeck coefficient S of the Bi_2Se_3 bulk were measured simultaneously using commercial equipment (ZEM-3, ULVAC-RIKO, Chigasaki, Kanagawa, Japan) in a He atmosphere from 300 to 540 K. The thermal conductivity κ of the Bi_2Se_3 bulk was calculated using the equation $\kappa = D \cdot C_p \cdot d$, where D is the thermal diffusivity, C_p is the specific heat, and d is the density of the sample. The thermal diffusivity D was examined via a laser-flash apparatus (NETZSCH, LFA 457, Selb, Germany), and the density d was obtained using the Archimedes method (presented in Figure S1, electronic supporting information (ESI)). The Seebeck coefficient S and the electrical resistivity ρ of an NW were measured using a conventional steady-state method in an Oxford cryostat. The NW thermal conductivity was measured using the 3ω method.

The TEM image (TEM; JEOL JEM-2100 at 200 kV, Tokyo, Japan) in Figure 1c reveals that the ordered hexagonal structure exhibiting lattice fringes of 0.21 nm gaps between the $[11\bar{2}0]$ planes were consistent with those of other lattice spacing measurements of Bi_2Se_3 NWs [47]. A corresponding selected area electron diffraction (SAED) pattern (Figure 1d) reveals that the Bi_2Se_3 NWs were high-quality single crystals that exhibited growth along the $[11\bar{2}0]$ direction. The chemical composition of the Bi_2Se_3 NW was examined using energy dispersive X-ray spectroscopy (EDS, JEOL, Tokyo, Japan); the EDS mapping shown in the inset of Figure 1e indicates the uniform spatial distribution of Bi and Se elements throughout the NW.

Figure 2 shows a SEM image of a Bi_2Se_3 NW ($d = 200$ nm) suspended on a Si_3N_4 microchip between 10 nm Ni/50 nm Au electrodes and a Pt/C electrical contact deposited by a focus ion beam (FIB). The sample used in this study showed nearly an ohmic contact. Subsequently, the microchip was used to determine the values of electrical resistivity ρ and S via four-point measurements.

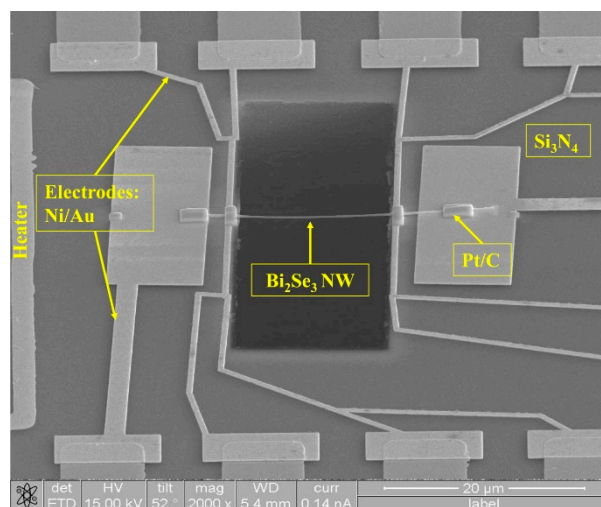


Figure 2. The SEM image of a single-crystal Bi_2Se_3 NW (diameter = 200 nm) placed on a Si_3N_4 microchip following electrode formation by using a FIB.

3.2. Characterization of Thermoelectric Properties

Figure 3a shows the temperature dependence of the electrical resistance at 290–320 K for a 200 nm Bi_2Se_3 NW that exhibited weak metallic conductivities. The σ of the NW at near room temperature was $1.50767 \times 10^5 \text{ S m}^{-1}$ (Figure 3b), which was approximately 55% lower than that of the Bi_2Se_3 bulk single-crystal ($2.7550 \times 10^5 \text{ S m}^{-1}$) [41] (Table 1). Furthermore, the surface scattering of charge carriers typically yields a reduced σ value [48]. However, the σ values of the Bi_2Se_3 NW at room temperature was higher than those reported in previous studies on the Bi_2Se_3 bulk [23–26,28,29,32], and even higher than that of the Bi_2Se_3 single-crystal made by Hor et al. [39], probably the result of the increased contribution of conduction surfaces up to 73% of the total electrical conduction upon decreasing the NW dimension via the high surface-to-volume ratio $s/v \sim 2 \text{ nm}^{-1}$ of the nanowires. A previous report [19] of electrical transport experiments on Bi_2Te_3 and $\text{Bi}_2\text{Se}_2\text{Te}$ nanowires in the range of 200–300 nm in diameter revealed that the two-dimensional TI surface channels contribute up to 30–70% of the total electrical conduction at surface-to-volume ratios of $s/v = 2\text{--}5 \times 10^{-2} \text{ nm}^{-1}$.

The S values with the negative sign obtained for the Bi_2Se_3 NW (Figure 3c) show that the Bi_2Se_3 NW is an n -type semiconductor, because electrons have much higher mobility than holes and dominate the transport [49,50]. This is reasonable because undoped Bi_2Se_3 is strongly n -type [51]. Furthermore, the room temperature S values for the n -type Bi_2Se_3 NW was $-51 \mu\text{VK}^{-1}$ for the 200 nm NW, the value was comparable to those typically reported by Greenaway and Harbeke for this material (i.e., in the -55 to $-73 \mu\text{VK}^{-1}$ range) [52], indicating that the Fermi level lay well inside the conduction band. The magnitude of the S smoothly increased as the temperature increased. This behavior was consistent with that expected of a metallically doped material. The magnitude of S for the NW tends to be zero when the temperature is decreased because S represents the entropy per electric charge and must decrease to zero at 0 K [15]. Figure 3d indicates the temperature dependence of the PF of Bi_2Se_3 NW, indicating that the PF increased as temperature increased; this can be attributed to the increase in the S with the temperature of the Bi_2Se_3 NW. The PF value of the 200 nm Bi_2Se_3 NW at room temperature was $39.32 \times 10^{-5} \text{ Wm}^{-1}\text{K}^{-2}$, which was higher than the PF of the Bi_2Se_3 bulk nanostructures [21–24,26,27,31]. The enhanced PF value is likely a result of enhanced electronic transport of the NW.

For semiclassical transport (metals or degenerate semiconductors) the carrier-density dependence of the thermopower is described by the Mott relation [53–55]:

$$S = \frac{8\pi^2 k_B^2 T}{3qh^2} m^* \left(\frac{\pi}{3n} \right)^{\frac{2}{3}} \quad (1)$$

where k_B is Boltzmann's constant, q is the electron charge, h is Planck's constant, T is the measurement temperature, m^* is the effective mass of the carrier ($m^* = 0.14 m_0$ in Bi_2Se_3) [56] and m_0 is the electron mass. This formula is valid for assessing metals or degenerate semiconductors that exhibit an n value in the range of 10^{18} to 10^{20} cm^{-3} [57,58]. The value of n is in the range of $1.26\text{--}1.35 \times 10^{19} \text{ cm}^{-3}$ at 290–320 K for the 200 nm NW (Figure 4), indicating that the NW is a degenerate semiconductor. This value is close to that calculated by Boechko et al. for n-type single crystals of a Bi_2Se_3 single crystal ($1\text{--}4 \times 10^{19} \text{ cm}^{-3}$) [59]. The value of n increased as the temperature increased, indicating the intrinsic condition [60], with the number of thermally generated carriers exceeding the number of donor carriers. The intrinsic carrier concentration in a material n_i is generally much smaller than the dopant carrier concentration at room temperature, but n_i ($=n \cdot p$) has a very strong temperature dependence:

$$n_i \propto T^{1.5} e^{-\frac{E_{g0}}{2kT}} \quad (2)$$

where E_{g0} is the energy band gap at $T = 0 \text{ K}$ [60].

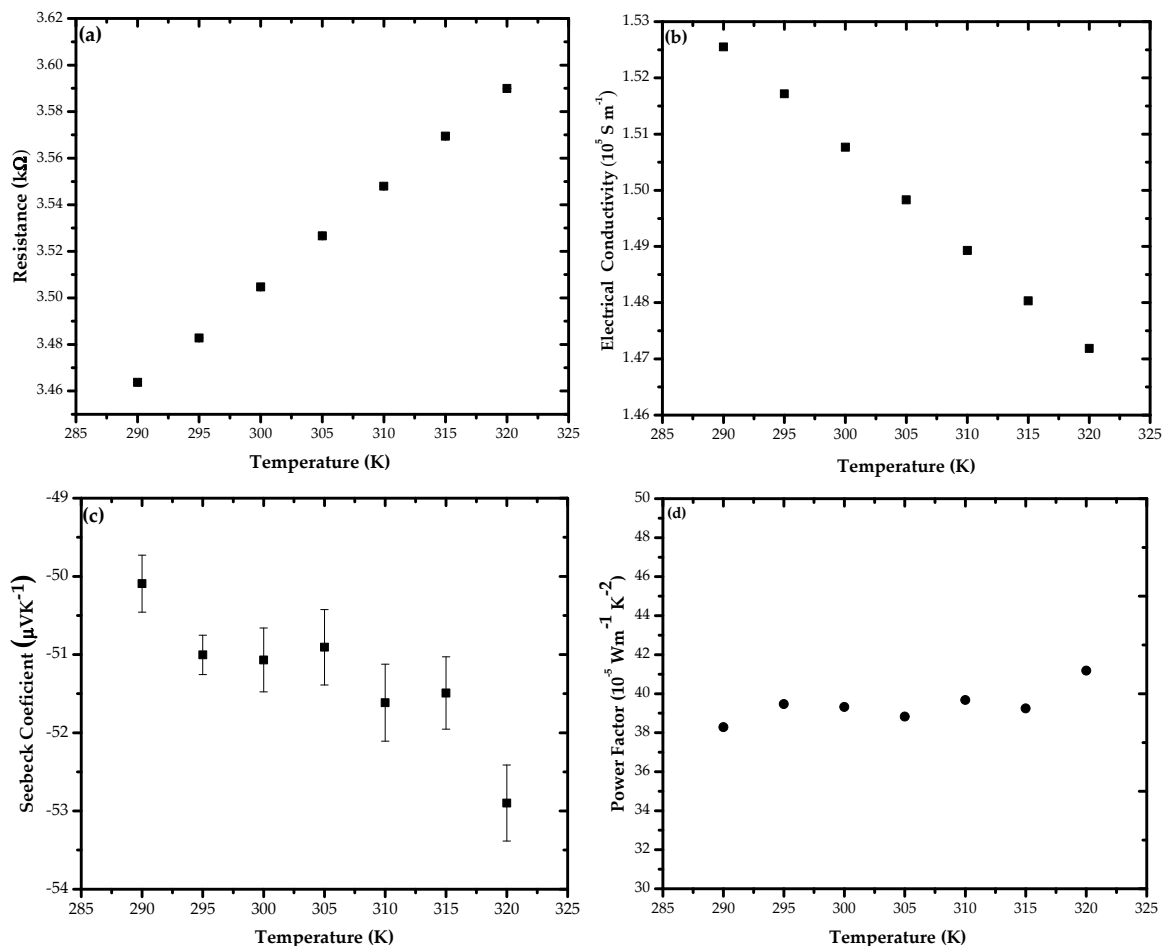


Figure 3. Temperature dependence regarding the (a) electrical resistance, (b) electrical conductivity, (c) TE power (S) and (d) power factor of the single-crystal Bi_2S_3 NW.

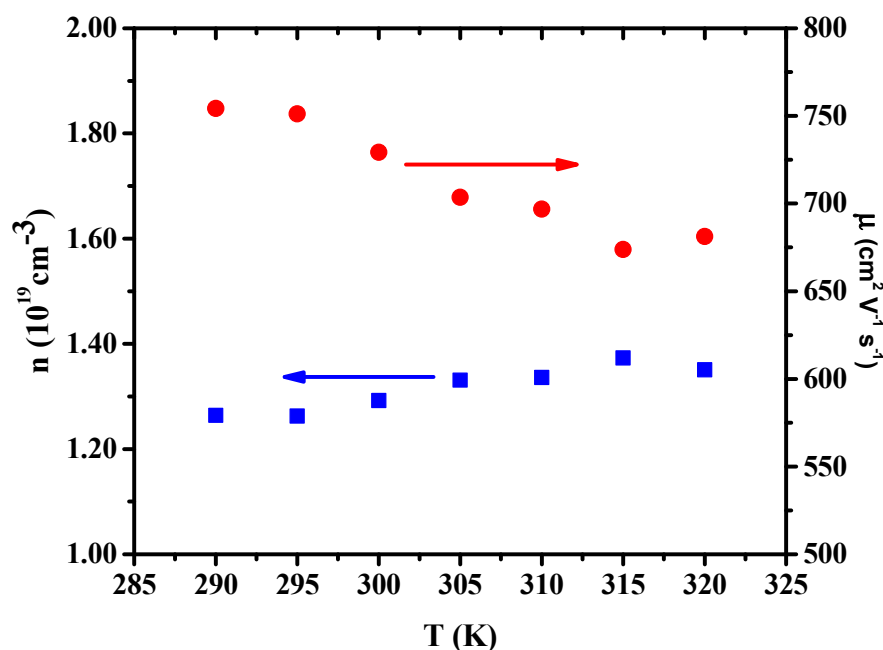


Figure 4. Temperature dependence of carrier concentration and carrier mobility for Bi₂Se₃ NW.

Figure 4 also depicts the calculated T dependences of carrier mobility μ for the Bi₂Se₃ NW. The μ value is obtained using the following equation:

$$\mu = \frac{1}{\rho n q} = \frac{\sigma}{n q} \quad (3)$$

Our calculated values of μ at 290–320 K were 754–681 cm² V⁻¹ s⁻¹ for the 200 nm NW; these values were much smaller than those of the Bi₂Se₃ bulk (approximately 920–1060 cm² V⁻¹ s⁻¹) [41], but higher than those reported by Le et al. [60] for Bi₂Se₃ TFs (7.2 ± 0.2 to 98.4 ± 0.5 cm² V⁻¹ s⁻¹). The μ values decreased as temperature increased because of the phonon concentration increase that caused increased scattering. Thus, lattice scattering reduced the carrier mobility at higher temperature. The mobility of a semiconductor depends on the impurity concentrations (including donor and acceptor concentrations), defect concentration, temperature, and electron and hole concentrations.

The primary factor involved in determining μ in the semiconductor is the scattering mechanism through the relation $\mu_j \propto T^\alpha$ [61]. Conduction carriers are scattered by acoustic phonons μ_l when $\alpha = -\frac{3}{2}$, whereas they are scattered by ionized impurities μ_i when $\alpha = \frac{3}{2}$. The μ values of the 200 nm Bi₂Se₃ NW continually decreased as the T increased, indicating that phonon scattering was dominant throughout the whole temperature range.

The thermal conductivity of Bi₂Se₃ NW was measured by the self-heating 3 ω method in the temperature range of 290–320 K. The 3 ω signal can be expressed as [62,63]:

$$V_{3\omega} = \frac{4I_0^3 L R R'}{\pi^4 \kappa S \sqrt{1 + (2\omega\gamma)^2}} \quad (4)$$

where I and ω are the amplitude and frequency of the alternating current applied on the nanowire, respectively; R and R' are the resistance and derivative of resistance at the corresponding temperature, respectively; κ is the thermal conductivity; S is the NW cross-section area; and γ is the characteristic thermal time constant. Figure 5a shows the current dependence of $V_{3\omega}$ at 300 K, demonstrating an I_0 dependence in an intermediate current range; one can see that $V_{3\omega}(I_0)$ followed the I_0^3 dependence well, in agreement with Equation (4). Figure 5b,c show the frequency dependencies of the amplitude and the

phase angle of $V_{3\omega}$ at 300 K, respectively, compared with the predicted functional forms (the solid lines). The fitting parameters for Figure 5a,b are shown in Tables S1 and S2, respectively.

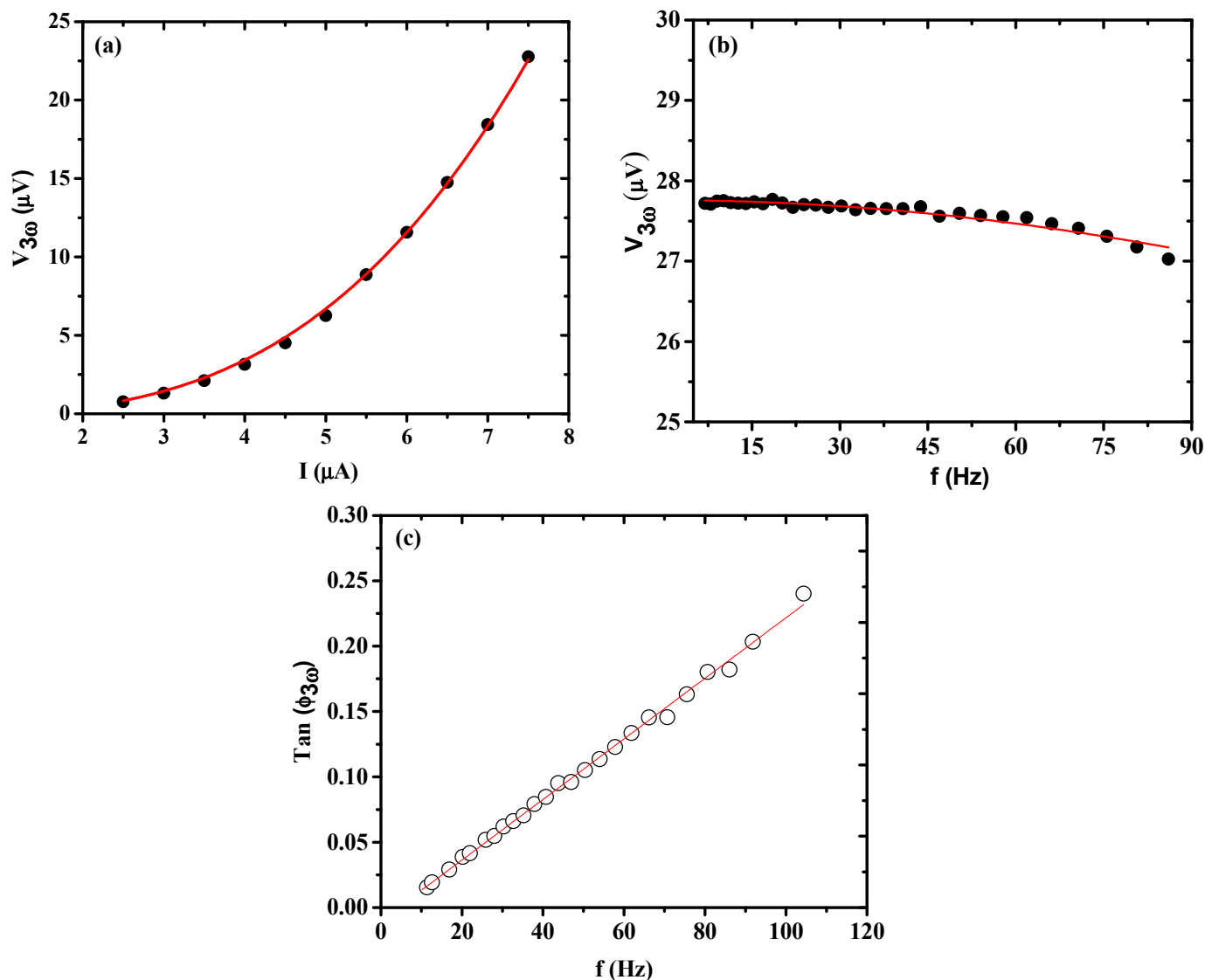


Figure 5. (a) The third harmonic voltage signal $V_{3\omega}$ as function of the extraction current amplitude I_0 . The solid line shows the cubic relationship of $V_{3\omega}$ and I_0 . (b) Frequency dependence of $V_{3\omega}$. The solid line is the predicted relation $V_{3\omega} \propto 1/\sqrt{1 + (2\omega\gamma)^2}$. (c) The frequency dependence of the phase angle of $V_{3\omega}$ at 300 K of Bi_2Se_3 NW; $d = 200$ nm.

By fitting the data in Figure 5a to equation $V_{3\omega} = \frac{4I_0^3 L R R'}{\pi^4 \kappa S}$ ($\omega\gamma \rightarrow 0$), we obtained the thermal conductivity κ , and the thermal time constant γ was ~ 2 ms at 300 K, comparable to a simple theoretical calculation of κ based on the Callaway model for nanostructured Bi_2Se_3 made by Li et al. [64,65]. It is known that phonon-boundary scattering can suppress the thermal conductivity in nanowires [66,67]. However, the data on a Bi_2Se_3 NW with $d = 200$ nm from the experimental κ values ($\kappa = 2.02$ to 2.09 $\text{W m}^{-1} \text{K}^{-1}$ at 290–320 K) as plotted in Figure 6a are in reasonable agreement with the Callaway model between the κ values of 300 nm ($\kappa > 2$ $\text{W m}^{-1} \text{K}^{-1}$) and 100 nm ($\kappa < 2$ $\text{W m}^{-1} \text{K}^{-1}$) [64]. The measured thermal conductivity, given by the κ value (κ is measured perpendicular to c plane) at $T = 300$ K of the NW (2.05 $\text{W m}^{-1} \text{K}^{-1}$) was $\sim 33\%$ lower than those for Bi_2Se_3 bulk single-crystal (2.96 $\text{W m}^{-1} \text{K}^{-1}$ or 3.1 $\text{W m}^{-1} \text{K}^{-1}$ in Table 1) [39,41].

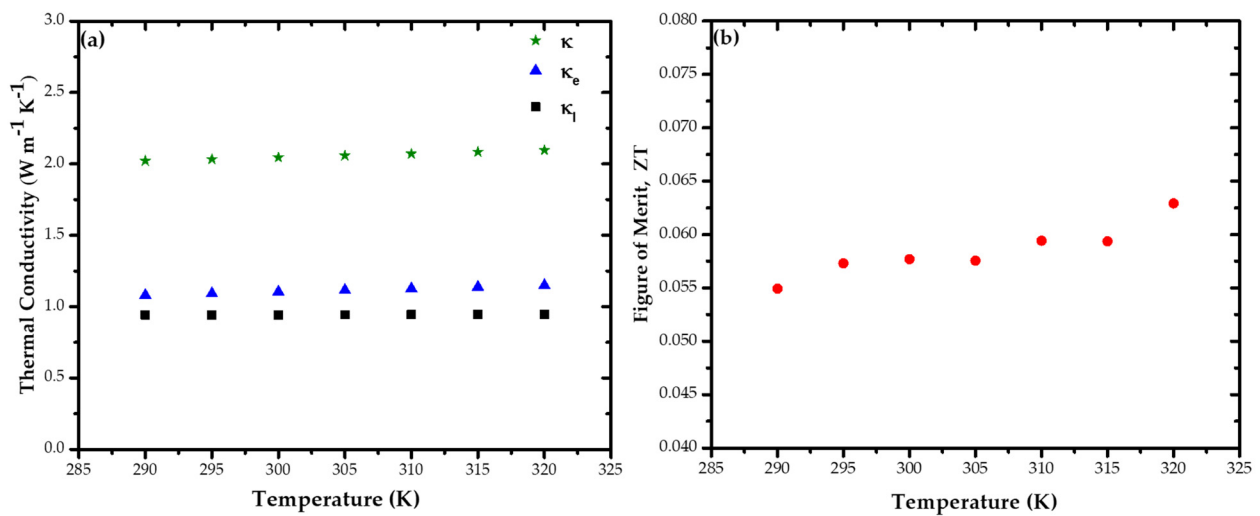


Figure 6. (a) Thermal conductivity κ , and (b) figure of merit ZT values of Bi_2Se_3 NW in the temperature range of 290 K to 320 K.

Table 1. The transport properties of Bi_2Se_3 nanowire and bulk at room temperature.

Sample *	S [$\mu\text{V K}^{-1}$]	Σ [S m^{-1}]	PF [$10^{-5} \text{ W m}^{-1}\text{K}^{-2}$]	κ $\text{W m}^{-1}\text{K}^{-1}$	ZT	Ref.
Bi_2Se_3	−53	38678	10.70	0.78	0.04	[26]
Bi_2Se_3	−115	212	2.80	0.75	0.01	[28]
$\text{Bi}_2\text{Se}_{2.83}$	−60	25000	9	0.55	0.05	[29]
Bi_2Se_3 Nanowire SC ($\varphi = 200 \text{ nm}$)	−51	150767	39.32	2.05	0.06	Our Work
Bi_2Se_3 Bulk SC	−62.10	259998	100	1.55	0.19	Our Work
Bi_2Se_3 Bulk SC	−190	47619	172	2.96	0.17	[39]
Bi_2Se_3 Bulk SC	−59	275500	95.90	3.1	0.09	[41]

* SC = single-crystalline.

The electronic thermal conductivity κ_e values of the Bi_2Se_3 NWs here were calculated according to the Wiedemann–Franz law:

$$\kappa_e = L\sigma T \quad (5)$$

where L is the Lorenz number ($2.44 \times 10^{-8} \text{ W } \Omega \text{ K}^{-2}$). When subtracting the κ_e values from the measured thermal conductivity, one obtains the phonon (or lattice) part of the thermal conductivity as $\kappa_l = \kappa - \kappa_e$. The temperature-dependent data for κ_l thus obtained are shown in Figure 6a. The obtained for κ_l and κ_e at 300 K for NWs were 29% and 37% lower than that of the Bi_2Se_3 bulk single-crystal ($\kappa_l = 1.33 \text{ W m}^{-1} \text{ K}^{-1}$ and $\kappa_e = 1.77 \text{ W m}^{-1} \text{ K}^{-1}$) [41]. The thermal conductivity was dominated by the electronic contribution in the 290–320 K range, although Birkholz and Rosi both reported a value for κ_l of Bi_2Se_3 bulk of between 2.0 and 2.4 $\text{W m}^{-1} \text{ K}^{-1}$ [51]. It was shown that the large surface-to-volume ratio s/v of nanowires could enhance phonon surface scattering and decrease κ_l .

Additionally, for this nanowire, ZT calculated from the obtained S , σ , and κ was approximately 0.06 at 300 K (Figure 6b). However, the ZT values of this nanowire were still higher than those of Bi_2Se_3 bulk used to construct nanostructures at 290–320 K, as reported previously [26,28,29]. Table 1 shows a summary of the transport properties of single-crystalline Bi_2Se_3 NW, compared with those reported Bi_2Se_3 bulk at room temperature. Our S , σ , and κ results of Bi_2Se_3 NW $d = 200 \text{ nm}$ were in reasonable agreement with a theoretical study [19]. This agreement indicates the high-quality crystallinity of the Bi_2Se_3 NWs grown by the stress-induced method.

4. Conclusions

The stress-induced method was applied to grow single-crystalline Bi_2Se_3 nanowires (NWs) from a Bi_2Se_3 TF on a SiO_2/Si substrate, offering an alternative technique for Bi_2Se_3 NWs synthesis without a catalyst. This technique had not been previously applied to

Bi_2Se_3 alloys. In this work, at room temperature, the Bi_2Se_3 nanowire (NW) ($d = 200$ nm) exhibited a PF of approximately $39.32 \times 10^{-5} \text{ W m}^{-1} \text{ K}^{-2}$, which was higher than that reported for Bi_2Se_3 bulk nanostructures; this discrepancy was mainly attributed to the electron-transport contribution of this NW. The measured thermal conductivity κ value of a NW was $2.05 \text{ W m}^{-1} \text{ K}^{-1}$, which was 31–34% lower than those for a Bi_2Se_3 bulk single crystal [39,41] because of the electron-scattering contribution. The figure of merit ZT value of Bi_2Se_3 NW rose up to approximately 0.06 at room temperature, in agreement with a theoretical study of the thermoelectric properties on a topological insulator of Bi_2Se_3 NWs [19]. Our results indicated that NWs grown using the stress-induced method yield high-quality single crystals.

Supplementary Materials: The following are available online at <https://www.mdpi.com/2079-4991/11/3/819/s1>, Figure S1: (a) Image of Bi_2Se_3 single-crystalline grown by the Bridgman method. (b) The measured thermoelectric properties were $-62.10 \mu \text{VK}^{-1}$, 259998 S m^{-1} , $1.55 \text{ W m}^{-1} \text{ K}^{-1}$, and 0.19 for the Seebeck coefficient (S), electrical conductivity (σ), thermal conductivity (κ) and figure of merit ZT , respectively, at room temperature, as shown in Table 1, Table S1: The fitting parameters of the third harmonic voltage signal $V3\omega$ as function of the extraction current amplitude I_0 for Figure 5a, Table S2: The fitting parameters of frequency dependence of $V3\omega$ for Figure 5b.

Author Contributions: Conceptualization, D. and Y.-Y.C.; methodology, D., P.-C.W. and P.-C.L.; software, D. and P.-C.L.; validation, D. and Y.-Y.C.; formal analysis, D., P.-C.L. and Y.-Y.C.; investigation, D., P.-C.L. and Y.-Y.C.; resources, D., P.-C.W. and P.-C.L.; data curation, D., P.-C.L. and Y.-Y.C.; writing—original draft preparation, D.; writing—review and editing, D., P.-C.L. and Y.-Y.C.; visualization, D.; project administration, P.-C.L. and Y.-Y.C.; supervision, Y.-Y.C.; funding acquisition, D. and Y.-Y.C., All authors have read and agreed to the published version of the manuscript.

Funding: This study was funded by the National Science Council of Taiwan (grant NSC 100-2112-M-001-019-MY3), and the publishing fee was supported by the Research Center for Electronics and Telecommunications (P2ET), Indonesian Institute of Sciences (LIPI).

Data Availability Statement: The data presented in this study are available on request from the corresponding author.

Acknowledgments: The authors wish to thank the Core Facilities for Nanoscience and Nanotechnology at the Institute of Physics of the Academia Sinica in Taiwan for providing technical support.

Conflicts of Interest: The authors declare no conflict of interest.

References

1. Boukai, A.I.; Bunimovich, Y.; Tahir-Kheli, J.; Yu, J.K.; Goddard, W.A.; Heath, J.R. Silicon nanowires as efficient thermoelectric materials. *Nature* **2008**, *451*, 168–171. [CrossRef]
2. Bubnova, O.; Khan, Z.U.; Malti, A.; Braun, S.; Fahlman, M.; Berggren, M.; Crispin, X. Optimization of the thermoelectric figure of merit in the conducting polymer poly(3,4-ethylenedioxythiophene). *Nat. Mater.* **2011**, *10*, 429–433. [CrossRef]
3. Hochbaum, A.I.; Chen, R.; Delgado, R.D.; Liang, W.; Garnett, E.C.; Najarian, M.; Majumdar, A.; Yang, P. Enhanced thermoelectric performance of rough silicon nanowires. *Nature* **2008**, *451*, 163–167. [CrossRef]
4. Minnich, A.J.; Dresselhaus, M.S.; Ren, Z.F.; Chen, G. Bulk nanostructured thermoelectric materials: Current research and future prospects. *Energy Environ. Sci.* **2009**, *2*, 466–479. [CrossRef]
5. Zhao, H.; Pokheral, M.; Zhu, G.; Chen, S.; Lukas, K.; Jie, Q.; Opeil, C.; Chen, G.; Ren, Z. Dramatic thermal conductivity reduction by nanostructures for large increase in thermoelectric figure-of-merit of FeSb_2 . *Appl. Phys. Lett.* **2011**, *99*, 2012–2015. [CrossRef]
6. Snyder, G.J.; Toberer, E.S. Complex thermoelectric materials. *Mater. Sustain. Energy Collect. Peer Rev. Res. Rev. Artic. Nat. Publ. Group* **2010**, *7*, 101–110.
7. Tritt, T.M.; Subramanian, M.A. Thermoelectric Materials, Phenomena and Applications: A Bird's Eye View. *MRS bulletin* **2006**, *31*, 188–198. [CrossRef]
8. Disalvo, F.J. Thermoelectric cooling and power generation. *Science* **1999**, *285*, 703–706. [CrossRef]
9. Tritt, T.M. Thermoelectric materials: Holey and Unholey Semiconductors. *Science* **1999**, *283*, 804–805. [CrossRef]
10. Rowe, D.M. *CRC Handbook of Thermoelectrics*; CRC Press: Danvers, MA, USA, 1995; ISBN 0849301467.
11. Dresselhaus, M.S.; Chen, G.; Tang, M.Y.; Yang, R.; Lee, H.; Wang, D.; Ren, Z.; Fleurial, J.P.; Gogna, P. New directions for low-dimensional thermoelectric materials. *Adv. Mater.* **2007**, *19*, 1043–1053. [CrossRef]
12. Mahan, G.D.; Sofo, J.O. The best thermoelectric. *Proc. Natl. Acad. Sci. USA* **1996**, *93*, 7436–7439. [CrossRef]

13. Lin, Y.M.; Sun, X.; Dresselhaus, M. Theoretical investigation of thermoelectric transport properties of cylindrical Bi nanowires. *Phys. Rev. B* **2000**, *62*, 4610–4623. [[CrossRef](#)]
14. Hicks, L.; Dresselhaus, M.S. Effect of quantum-well structures on the thermoelectric figure of merit. *Phys. Rev. B* **1993**, *47*, 12727. [[CrossRef](#)]
15. Boukai, A.; Xu, K.; Heath, J.R. Size-dependent transport and thermoelectric properties of individual polycrystalline bismuth nanowires. *Adv. Mater.* **2006**, *18*, 864–869. [[CrossRef](#)]
16. Slack, G. New Materials and Performance Limits for Thermoelectric Cooling. In *CRC Handbook Thermoelectrics*; CRC Press: Danvers, MA, USA, 1995.
17. Mishra, S.K.; Satpathy, S.; Jepsen, O. Electronic structure and thermoelectric properties of bismuth telluride and bismuth selenide. *J. Phys. Condens. Matter* **1997**, *9*, 461–470. [[CrossRef](#)]
18. Al Bayaz, A.; Giani, A.; Foucaran, A.; Pascal-Delannoy, F.; Boyer, A. Electrical and thermoelectrical properties of Bi₂Se₃ grown by metal organic chemical vapour deposition technique. *Thin Solid Films* **2003**, *441*, 1–5. [[CrossRef](#)]
19. Gooth, J.; Glusckhe, J.G.; Zierold, R.; Leijnse, M.; Linke, H.; Nielsch, K. Thermoelectric performance of classical topological insulator nanowires. *Semicond. Sci. Technol.* **2015**, *30*, 015015. [[CrossRef](#)]
20. Watanabe, K.; Sato, N.; Miyaoka, S. New optical recording material for video disc system. *J. Appl. Phys.* **1983**, *54*, 1256–1260. [[CrossRef](#)]
21. Waters, J.; Crouch, D.; Raftery, J.; O'Brien, P. Deposition of bismuth chalcogenide thin films using novel single-source precursors by metal-organic chemical vapor deposition. *Chem. Mater.* **2004**, *16*, 3289–3298. [[CrossRef](#)]
22. Venkatasubramanian, R.; Siivola, E.; Colpitts, T.; O'Quinn, B. Thin-film thermoelectric devices with high room-temperature figures of merit. *Nature* **2001**, *413*, 597–602. [[CrossRef](#)] [[PubMed](#)]
23. Xu, H.; Chen, G.; Jin, R.; Pei, J.; Wang, Y.; Chen, D. Hierarchical Bi₂Se₃ microrods: Microwave-assisted synthesis, growth mechanism and their related properties. *Cryst. Eng. Comm.* **2013**, *15*, 1618–1625. [[CrossRef](#)]
24. Xu, H.; Chen, G.; Jin, R.; Chen, D.; Wang, Y.; Pei, J.; Zhang, Y.; Yan, C.; Qiu, Z. Microwave-assisted synthesis of Bi₂Se₃ ultrathin nanosheets and its electrical conductivities. *Cryst. Eng. Comm.* **2014**, *16*, 3965–3970. [[CrossRef](#)]
25. Lin, Y.F.; Chang, H.W.; Lu, S.Y.; Liu, C.W. Preparation, characterization, and electrophysical properties of nanostructured BiPO₄ and Bi₂Se₃ derived from a structurally characterized, single-source precursor Bi[Se₂P(OiPr)₂]₃. *J. Phys. Chem. C* **2007**, *111*, 18538–18544. [[CrossRef](#)]
26. Bai, T.; Li, C.; Liang, D.; Li, F.; Jin, D.; Shi, Z.; Feng, S. Synthesis of various metal selenide nanostructures using the novel selenium precursor 1,5-bis(3-methylimidazole-2-selone)pentane. *Cryst. Eng. Comm.* **2013**, *15*, 6483–6490. [[CrossRef](#)]
27. Manjare, S.T.; Yadav, S.; Singh, H.B.; Butcher, R.J. Redox reaction between main-group elements (Te, Sn, Bi) and N-Heterocyclic-carbene-derived selenium halides: A facile method for the preparation of monomeric halides. *Eur. J. Inorg. Chem.* **2013**, *2013*, 5344–5357. [[CrossRef](#)]
28. Kadel, K.; Kumari, L.; Li, W.Z.; Huang, J.Y.; Provencio, P.P. Synthesis and thermoelectric properties of Bi₂Se₃ nanostructures. *Nanoscale Res. Lett.* **2011**, *6*, 57. [[CrossRef](#)] [[PubMed](#)]
29. Min, Y.; Roh, J.W.; Yang, H.; Park, M.; Kim, S.I.; Hwang, S.; Lee, S.M.; Lee, K.H.; Jeong, U. Surfactant-free scalable synthesis of Bi₂Te₃ and Bi₂Se₃ nanoflakes and enhanced thermoelectric properties of their nanocomposites. *Adv. Mater.* **2013**, *25*, 1425–1429. [[CrossRef](#)] [[PubMed](#)]
30. Sun, Z.; Liufu, S.; Chen, L. Synthesis and characterization of nanostructured bismuth selenide thin films. *Dalt. Trans.* **2010**, *39*, 10883–10887. [[CrossRef](#)] [[PubMed](#)]
31. Giani, A.; Al Bayaz, A.; Foucaran, A.; Pascal-Delannoy, F.; Boyer, A. Elaboration of Bi₂Se₃ by metalorganic chemical vapour deposition. *J. Cryst. Growth* **2002**, *236*, 217–220. [[CrossRef](#)]
32. Alegria, L.D.; Schroer, M.D.; Chatterjee, A.; Poirier, G.R.; Pretko, M.; Patel, S.K.; Petta, J.R. Structural and electrical characterization of Bi₂Se₃ nanostructures grown by metal-organic chemical vapor deposition. *Nano Lett.* **2012**, *12*, 4711–4714. [[CrossRef](#)]
33. Sun, Y.; Cheng, H.; Gao, S.; Liu, Q.; Sun, Z.; Xiao, C.; Wu, C.; Wei, S.; Xie, Y. Atomically thick bismuth selenide freestanding single layers achieving enhanced thermoelectric energy harvesting. *J. Am. Chem. Soc.* **2012**, *134*, 20294–20297. [[CrossRef](#)]
34. Checkelsky, J.G.; Hor, Y.S.; Cava, R.J.; Ong, N.P. Bulk band gap and surface state conduction observed in voltage-tuned crystals of the topological insulator Bi₂Se₃. *Phys. Rev. Lett.* **2011**, *106*, 4–7. [[CrossRef](#)] [[PubMed](#)]
35. Hong, S.S.; Kundhikanjana, W.; Cha, J.J.; Lai, K.; Kong, D.; Meister, S.; Kelly, M.A.; Shen, Z.X.; Cui, Y. Ultrathin topological insulator Bi₂Se₃ nanoribbons exfoliated by atomic force microscopy. *Nano Lett.* **2010**, *10*, 3118–3122. [[CrossRef](#)]
36. Janiček, P.; Drašar, Č.; Beneš, L.; Lošták, P. Thermoelectric properties of TI-doped Bi₂Se₃ single crystals. *Cryst. Res. Technol.* **2009**, *44*, 505–510. [[CrossRef](#)]
37. King, M.D.; Blanton, T.N.; Mixture, S.T.; Korter, T.M. Prediction of the unknown crystal structure of creatine using fully quantum mechanical methods. *Cryst. Growth Des.* **2011**, *11*, 5733–5740. [[CrossRef](#)]
38. Kašparová, J.; Drašar, Č.; Krejčová, A.; Beneš, L.; Lošták, P.; Chen, W.; Zhou, Z.; Uher, C. n-type to p-type crossover in quaternary Bi_xSb_yPb_zSe₃ single crystals. *J. Appl. Phys.* **2005**, *97*, 103720. [[CrossRef](#)]
39. Hor, Y.S.; Richardella, A.; Roushan, P.; Xia, Y.; Checkelsky, J.G.; Yazdani, A.; Hasan, M.Z.; Ong, N.P.; Cava, R.J. P-type Bi₂Se₃ for topological insulator and low-temperature thermoelectric applications. *Phys. Rev. B* **2009**, *79*, 195208. [[CrossRef](#)]
40. Qiu, X.; Austin, L.N.; Muscarella, P.A.; Dyck, J.S.; Burda, C. Nanostructured Bi₂Se₃ films and their thermoelectric transport properties. *Angew. Chem. Int. Ed.* **2006**, *45*, 5656–5659. [[CrossRef](#)]

41. Navrátil, J.; Horák, J.; Plecháček, T.; Kamba, S.; Lošťák, P.; Dyck, J.S.; Chen, W.; Uher, C. Conduction band splitting and transport properties of Bi₂Se₃. *J. Solid State Chem.* **2004**, *177*, 1704–1712. [[CrossRef](#)]
42. Dedi; Lee, P.C.; Chien, C.H.; Dong, G.P.; Huang, W.C.; Chen, C.L.; Tseng, C.M.; Harutyunyan, S.R.; Lee, C.H.; Chen, Y.Y. Stress-induced growth of single-crystalline lead telluride nanowires and their thermoelectric transport properties. *Appl. Phys. Lett.* **2013**, *103*, 1–6. [[CrossRef](#)]
43. Dedi; Chien, C.H.; Hsiung, T.C.; Chen, Y.C.; Huang, Y.C.; Lee, P.C.; Lee, C.H.; Chen, Y.Y. Structural, electronic transport and magnetoresistance of a 142nm lead telluride nanowire synthesized using stress-induced growth. *AIP Adv.* **2014**, *4*, 1–7. [[CrossRef](#)]
44. Cheng, Y.T.; Weiner, A.M.; Wong, C.A.; Balogh, M.P.; Lukitsch, M.J. Stress-induced growth of bismuth nanowires. *Appl. Phys. Lett.* **2002**, *81*, 3248–3250. [[CrossRef](#)]
45. Shim, W.; Ham, J.; Lee, K.; Jeung, W.Y.; Johnson, M.; Lee, W. On-film formation of Bi nanowires with extraordinary electron mobility. *Nano Lett.* **2009**, *9*, 18–22. [[CrossRef](#)]
46. Chen, X.; Zhou, H.D.; Kiswandhi, A.; Miotkowski, I.; Chen, Y.P.; Sharma, P.A.; Lima Sharma, A.L.; Hekmaty, M.A.; Smirnov, D.; Jiang, Z. Thermal expansion coefficients of Bi₂Se₃ and Sb₂Te₃ crystals from 10 K to 270 K. *Appl. Phys. Lett.* **2011**, *99*, 12–15. [[CrossRef](#)]
47. Kong, D.; Randel, J.C.; Peng, H.; Cha, J.J.; Meister, S.; Lai, K.; Chen, Y.; Shen, Z.X.; Manoharan, H.C.; Cui, Y. Topological insulator nanowires and nanoribbons. *Nano Lett.* **2010**, *10*, 329–333. [[CrossRef](#)] [[PubMed](#)]
48. Wang, D.; Sheriff, B.A.; Heath, J.R. Complementary symmetry silicon nanowire logic: Power-efficient inverters with gain. *Small* **2006**, *2*, 1153–1158. [[CrossRef](#)] [[PubMed](#)]
49. Partin, D.L. Growth and characterization of epitaxial bismuth films. *J. Vac. Sci. Technol. B Microelectron. Nanom. Struct.* **1989**, *7*, 348. [[CrossRef](#)]
50. De Kuijper, A.H.; Bisschop, J. Temperature dependence of concentrations and mobilities in thin bismuth films. *Thin Solid Films* **1983**, *110*, 99–106. [[CrossRef](#)]
51. Nolas, G.S.; Sharp, J.; Goldsmid, J. *Thermoelectrics: Basic Principles and New Materials Developments*; Springer-Verlag: Berlin/Heidelberg, Germany, 2013; Volume 45, ISBN 9781461257080.
52. Greenaway, D.L.; Harbeke, G. Band structure of bismuth telluride, bismuth selenide and their respective alloys. *J. Phys. Chem. Solids* **1965**, *26*, 1585–1604. [[CrossRef](#)]
53. Dedi; Idayanti, N.; Lee, P.-C.; Lee, C.-H.; Chen, Y.-Y. Thermoelectric power of single crystalline lead telluride nanowire. *J. Phys. Conf. Ser.* **2016**, *776*, 012046. [[CrossRef](#)]
54. Kim, D.; Syers, P.; Butch, N.P.; Paglione, J.; Fuhrer, M.S. Ambipolar surface state thermoelectric power of topological insulator Bi₂Se₃. *Nano Lett.* **2014**, *14*, 1701–1706. [[CrossRef](#)] [[PubMed](#)]
55. Cutler, M.; Mott, N.F. Observation of anderson localization in an electron gas. *Phys. Rev.* **1969**, *181*, 1336–1340. [[CrossRef](#)]
56. Wang, Z.; Lin, T.; Wei, P.; Liu, X.; Dumas, R.; Liu, K.; Shi, J. Tuning carrier type and density in Bi₂Se₃ by Ca-doping. *Appl. Phys. Lett.* **2010**, *97*, 2012–2015. [[CrossRef](#)]
57. Horák, J.; Navrátil, J.; Starý, Z. Lattice point defects and free-carrier concentration in Bi_{2+x}Te₃ and Bi_{2+x}Se₃ crystals. *J. Phys. Chem. Solids* **1992**, *53*, 1067–1072. [[CrossRef](#)]
58. Lee, C.H.; Yi, G.C.; Zuev, Y.M.; Kim, P. Thermoelectric power measurements of wide band gap semiconducting nanowires. *Appl. Phys. Lett.* **2009**, *94*, 1–4. [[CrossRef](#)]
59. Wolpert, D.; Ampadu, P. *Managing Temperature Effects in Nanoscale Adaptive Systems*; Hardcover; Springer-Verlag: New York, NY, USA, 2012; Volume XXII, pp. 1–174, ISBN 978-1-4614-0747-8.
60. Le, P.H.; Liao, C.N.; Luo, C.W.; Lin, J.Y.; Leu, J. Thermoelectric properties of bismuth-selenide films with controlled morphology and texture grown using pulsed laser deposition. *Appl. Surf. Sci.* **2013**, *285*, 657–663. [[CrossRef](#)]
61. Sze, S.M.; Ng, K.K. *Physics of Semiconductor Devices*, 3rd ed.; Wiley: Danvers, MA, USA, 2007; ISBN 978-0-471-14323-9.
62. Lu, L.; Yi, W.; Zhang, D.L. 3 Ω method for specific heat and thermal conductivity measurements. *Rev. Sci. Instrum.* **2001**, *72*, 2996–3003. [[CrossRef](#)]
63. Dedi; Primadona, I.; Lee, P.C.; Chien, C.H.; Chen, Y.Y. Structural and Thermoelectric Properties Characterization of Individual Single-Crystalline Nanowire. In *Impact of Thermal Conductivity on Energy Technologies*; Shahzad, A., Ed.; IntechOpen: London, UK, 2018; pp. 149–166, ISBN 978-1-78923-673-6.
64. Li, G.; Liang, D.; Qiu, R.L.J.; Gao, X.P.A. Thermal conductivity measurement of individual Bi₂Se₃ nano-ribbon by self-heating three-ω method. *Appl. Phys. Lett.* **2013**, *102*, 043104. [[CrossRef](#)]
65. Callaway, J. Model for lattice thermal conductivity at low temperatures. *Phys. Rev.* **1959**, *113*, 1046–1051. [[CrossRef](#)]
66. Zhou, J.; Jin, C.; Seol, J.H.; Li, X.; Shi, L. Thermoelectric properties of individual electrodeposited bismuth telluride nanowires. *Appl. Phys. Lett.* **2005**, *87*, 133109. [[CrossRef](#)]
67. Li, D.; Wu, Y.; Kim, P.; Shi, L.; Yang, P.; Majumdar, A. Thermal conductivity of individual silicon nanowires. *Appl. Phys. Lett.* **2003**, *83*, 2934–2936. [[CrossRef](#)]